LAWRENCE
LIVERMORE
NATIONAL
LABORATORY

UCRL-JC-134118

Modeling Large-Strain, High-Rate Deformation in Metals

D. R. Lesuer, G. J. Kay, M. M. LeBlanc

July 20, 2001

Third Biennial Tri-Laboratory Engineering Conference
Modeling and Simulation, Pleasanton, CA,
November 3-5, 1999

MODELING LARGE STRAIN, HIGH RATE DEFORMATION IN METALS*

D.R. Lesuer, G.J. Kay, M.M. LeBlanc

Lawrence Livermore National Laboratory, L-342, Livermore, CA 94551

Abstract

The large strain deformation response of 6061-T6 and Ti-6Al-4V has been evaluated over a range in strain rates from 10^{-4} s^{-1} to over 10^{4} s^{-1}. The results have been used to critically evaluate the strength and damage components of the Johnson-Cook (JC) material model. A new model that addresses the shortcomings of the JC model was then developed and evaluated. The model is derived from the rate equations that represent deformation mechanisms active during moderate and high rate loading. Another model that accounts for the influence of void formation on yield and flow behavior of a ductile metal (the Gurson model) was also evaluated. The characteristics and predictive capabilities of these models are reviewed.

* This work was performed under the auspices of the U.S. Department of Energy by the University of CA Lawrence Livermore National Laboratory under Contract No. W-7405-ENG-48.

Introduction

Background

Many modeling problems involving structural materials involve accurately representing the high rate deformation response. Examples include the modeling of material processing operations as well as the in-service performance of materials. Typical material processing operations, in which high rate deformation is observed, include material cutting, numerous forming operations (including rolling and forging) and material polishing. Typical in-service performance problems, in which high rate deformation is observed, include the ballistic penetration and perforation of armor materials, the crash response of automobiles and various accident problems involving aerospace structures. Many of these problems are difficult to accurately model. Much of this difficulty arises from the large strains and adiabatic heat produced which, in turn, causes increases in temperature with resulting changes in material microstructure, material properties and deformation mechanisms. Large changes in strain rate are also produced. In addition, deformation can produce instabilities in the form of adiabatic shear bands. Voids can also be produced that, in turn, can influence flow behavior and serve as a pre-cursor to fracture. Thus, accurate material models are necessary for understanding complex deformation behavior (and strength) as well as failure response.

Objectives

Material models which can adequately represent the deformation response during high rate loading must account for large strains (and the resulting strain hardening or softening), as well as large changes in strain rate and temperature. Several models have been developed which can represent, to varying degrees, the high rate deformation response of materials. Examples include models by Johnson-Cook (JC) [1-3], Zerilli-Armstrong (ZA) [4-6], and Follansbee-Kocks (mechanical threshold stress model) [7]. Several of these models have been introduced into finite element codes (e.g. DYNA3D). Of these models, the JC model is much more widely used. The JC model was developed during the 1980's to study impact, ballistic penetration and explosive detonation problems. The model has proven to be very popular and has been extensively used by a number of national laboratories, military laboratories and private industry to study high rate, large strain problems. The reasons for the popularity of this model include the simple form of the constitutive equations and the availability of constants used in the equations for a number of materials. The JC material model also has a cumulative damage law which can be used to assess failure.

In this paper, we examine the JC model and its ability to represent the large strain deformation behavior of two important structural materials - an $\alpha-\beta$ titanium alloy (Ti-6Al-4V) and a moderate strength aluminum alloy (6061-T6). The model has been evaluated over a range of strain rates from 10^{-4} s^{-1} to over 10^{4} s^{-1}. The damage law was also evaluated for its ability to predict failure in these materials. A new model is then developed and evaluated that addresses some of the shortcomings observed with the JC model. The model is derived from the rate equations that represent deformation mechanisms active during moderate and high rate loading. Another model that accounts for the influence of void formation on yield and flow behavior of a ductile metal (the Gurson model [8]) was also evaluated. The characteristics and predictive capabilities of these models are then reviewed.

Materials, Experiments and Results

The materials used in this study were obtained from commercial sources. The 6061 alloy was received as a hot, cross-rolled plate in the T6 temper. The Ti-6Al-4V alloy was processed according to the AMS 4911 specification, which produced an equiaxed alpha and transformed beta microstructure.

High rate testing was done in both compression and tension using the split Hopkinson pressure bar technique and data was obtained at strain rates of 10^3 - 10^4 s^{-1}. In the compression tests, the strain histories for the incident and transmitted waves in the elastic pressure bars were measured and analyzed to determine the nominal stress - strain - strain rate response of the sample. In the tension tests, the strain history in the elastic pressure bars were used to obtain the stress-time response of the sample. The strain and strain rate behavior of the sample was obtained from high speed photographic images derived from a framing camera.

The true stress-true strain data for 6061-T6 aluminum obtained in tension and compression is shown in Fig. 1. The experiments in tension were conducted at a strain rate of 8000 s^{-1}, and samples were tested with the tensile axis parallel to the longitudinal and transverse orientations in the plate. The experiments in compression were conducted at a strain rate of 4000 s^{-1}, and samples were tested with the compression axis parallel to the longitudinal, transverse and through-thickness orientations in the plate. Data for "elastic" loading of the sample can not be obtained in these tests due to wave propagation effects. The stress-strain data shown in Fig. 1 can be considered valid once the samples have yielded plastically, which is accompanied by stress and strain rate uniformity in the sample. The data for the different orientations of testing show that in both tension and compression the stress-strain response is highly isotropic. This is especially true in compression, in which the curves for the three orientations fall virtually on top of one another. The compression samples deformed to the limits of the experiment without failure, while the tension samples failed after a strain of .26.

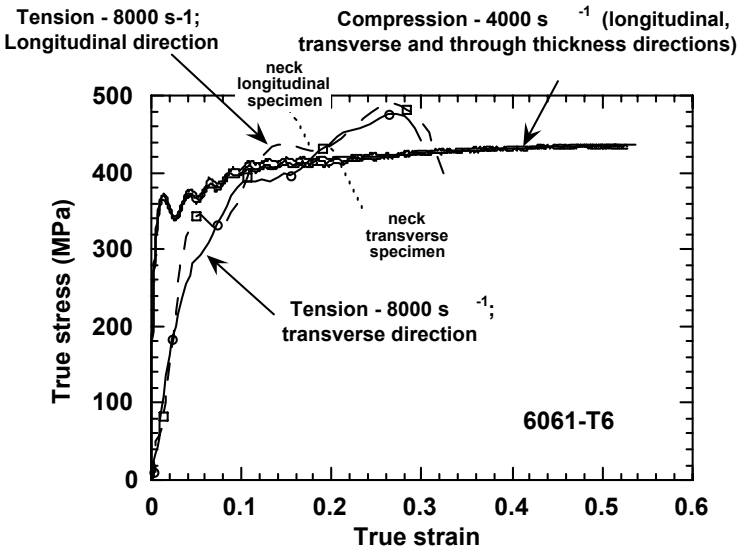

Figure 1. True stress-true strain data for 6061-T6 aluminum obtained in tension and compression with the split Hopkinson pressure bar apparatus. The experiments in tension were conducted in two different orientations and a strain rate of 8000 s^{-1}. The experiments in compression were conducted in three different orientations and a strain rate of 4000 s^{-1}.

Johnson-Cook Material Model

Background

The JC model is empirically based and represents the flow stress with an equation of the form,

$$\sigma = [A + B\varepsilon^n][1 + C\ln\dot{\varepsilon}^*][1 - T^{*m}] \quad (1)$$

where σ is the effective stress, ε is the effective plastic strain, $\dot{\varepsilon}^*$ is the normalized effective plastic strain rate (typically normalized to a strain rate of 1.0 s^{-1}), T^* is the homologous temperature, n is the work hardening exponent and A, B, C and m are constants. The values of A, B, C, n and m are determined from an empirical fit of flow stress data (as a function of strain, strain rate and temperature) to Eqn. (1). For high rate deformation problems, we can assume that an arbitrary percentage of the plastic work done during deformation produces heat in the deforming material. For many materials, 100% of the plastic work becomes heat in the material. Thus the temperature used in Eqn. (1) can be derived from the increase in temperature according to the following expression

$$\Delta T = \frac{\alpha B}{\rho c (n+1)}\varepsilon^{n+1} \quad (2)$$

where ΔT is the temperature increase, α is the percentage of plastic work transformed to heat, c is the heat capacity and ρ is the density.

Fracture in the JC material model is derived from the following cumulative damage law

$$D = \Sigma \frac{\Delta\varepsilon}{\varepsilon_f} \quad (3)$$

in which

$$\varepsilon_f = [D_1 + D_2\exp(D_3\sigma^*)][1+D_4\ln\dot{\varepsilon}^*][1+D_5T^*] \quad (4)$$

where $\Delta\varepsilon$ is the increment of effective plastic strain during an increment in loading and σ^* is the mean stress normalized by the effective stress. The parameters D_1, D_2, D_3, D_4 and D_5 are constants. Failure is assumed to occur when D = 1. The current failure strain in the problem (ε_f) is thus a function of mean stress, strain rate and temperature. The constants for the JC model used in the evaluations in the next section are given in Table 1

Table 1
Johnson-Cook constants for Ti-6Al-4V and 6061-T6

	A (MPa)	B (MPa)	n	C	m	D_1	D_2	D_3	D_4	D_5
6061-T6	324	114	.42	.002	1.34	-0.77	1.45	-0.47	0.0	1.60
Ti-6Al-4V	862	331	.34	.012	.8	-0.09	0.25	-0.5	.014	3.87

Model evaluation

The adiabatic stress-strain behavior for the 6061-T6 alloy predicted by the JC material model is shown in Fig. 2 for loading in tension, compression and shear. The cumulative damage predicted by the failure model is also shown in the figure, and the failure strains for the three stress states are indicated on the stress-strain curve. The three stress states show different damage curves because of the influence of the mean stress term on ε_f in Eqn (4). The stress-strain response predicted by the material model is compared against the experimental data in both tension and compression in Fig. 3. The yield strength predicted by the JC model correlates very well with the experimental results. However, the experimental stress-strain curves work harden at a higher rate. This is not a fundamental shortcoming of the model, since higher work hardening rates are possible with larger values of B and n in Eqn. (1). The failure strain in tension as predicted by the JC material model (ε_f = .52) is significantly higher than obtained experimentally (ε_f = .26). This is a significant difference and the physical origins of this discrepancy need to be understood. However, detailed studies of failure models are outside the scope of this paper.

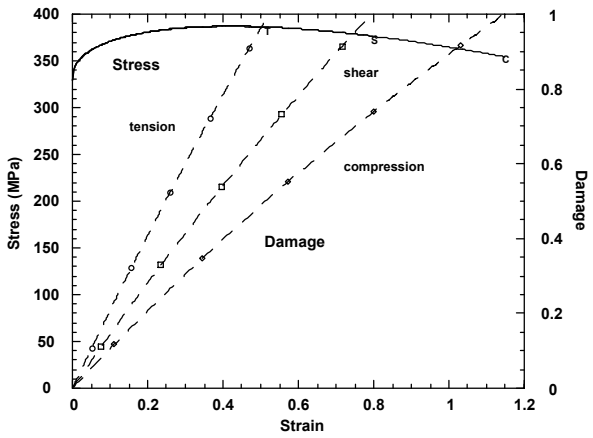

Figure 2. Adiabatic true stress-true strain behavior for 6061-T6 at a strain rate of 6000 s^{-1} predicted by the Johnson-Cook material model. Results are presented for loading in tension, compression and shear. The cumulative damage predicted by the material model is also shown. The failure point along the stress-strain curve is shown for tension (T), shear (S) and compression (C).

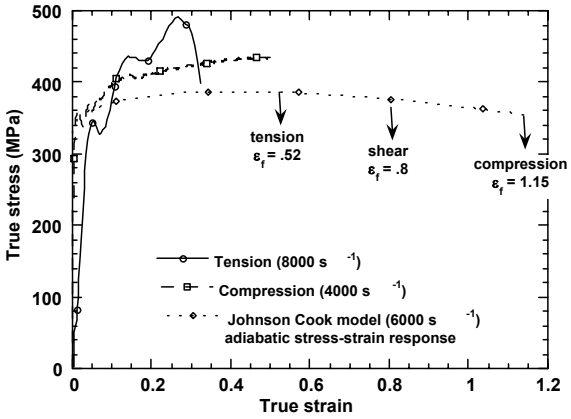

Figure 3. Comparison between the stress-strain behavior predicted by the JC material model and experimental data for the 6061-T6 alloy.

The stress-strain rate response for the 6061-T6 alloy is compared against the predictions of the JC model in Fig. 4. Data was obtained from the work of Nicholas [9] as well as the results of this study. Here significant deviations between model predictions and experimental results are evident. The experimental data shows a dramatic increase in strength above a strain rate of 10^3 s^{-1}. This increase in strength has been observed in a number of metals [10] and is generally recognized as resulting from a change in deformation mechanism. At lower strain rates, the deformation rate is controlled by the cutting or by-passing of discrete obstacles by dislocations. At higher rates, the deformation rate is controlled by phonon or electron drag on moving dislocations. These two mechanisms are represented by different deformation rate equations, which produces the dramatic change in behavior on going from low strain rates to high strain rates. Such dramatic changes in behavior are outside the scope of the JC model. We present a model in the next section which accounts for these mechanism changes.

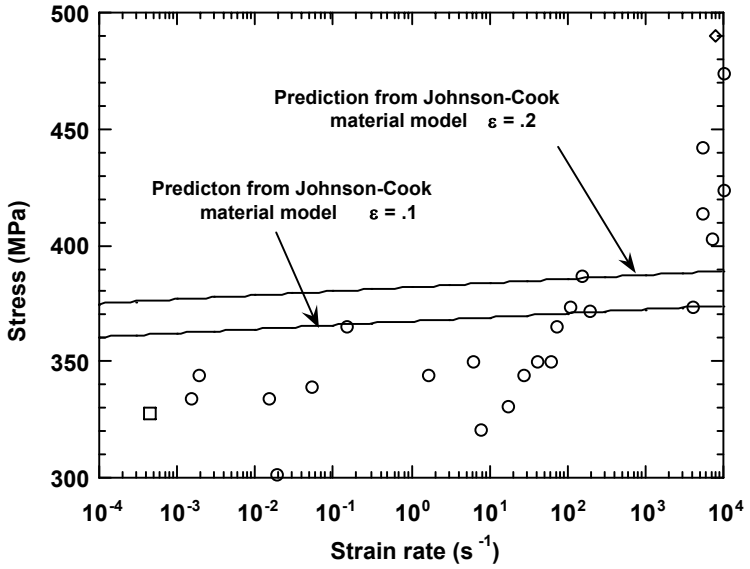

Figure 4. Comparison between the stress-strain rate behavior predicted by the JC material model and experimental data for the 6061-T6 alloy. Experimental data was derived from a compilation of ultimate tensile strength results from this study and data from reference 9.

The predictions of the JC model for the Ti-6Al-4V alloy are shown in Fig. 5 and compared against experimental data in Figs. 6 and 7. Data in Figs. 6 and 7 were obtained from the work of Wulf [11], Meyer [12] and Follansbee and Gray [13]. The same capabilities and limitations of the material model that were observed for the 6061-T6 alloy were noted for the Ti-6Al-4V alloy. The model can adequately represent work hardening behavior in both materials. The most serious limitation was its inability to predict variations of flow stress with strain rate as shown in Fig. 7. The failure model predicted the correct ductility in tension for the Ti-6Al-4V alloy (ε_f = .15) but, in compression, the model predicted a significantly higher ductility than observed experimentally.

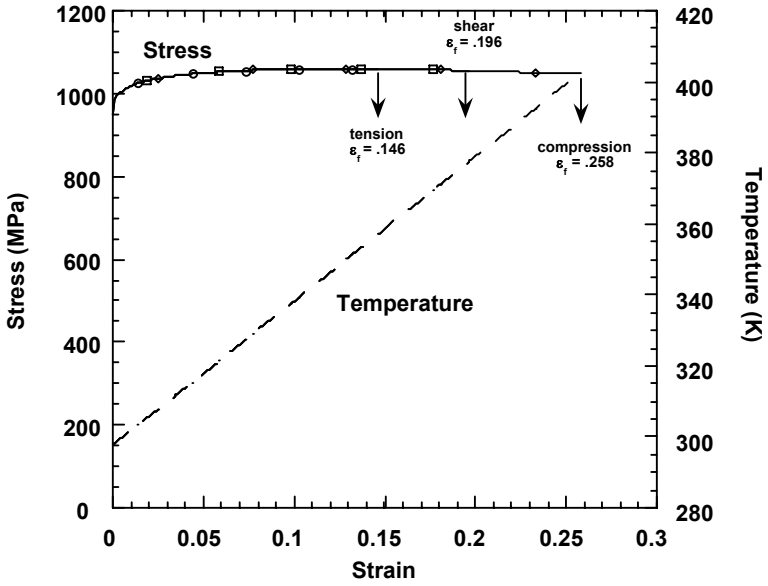

Figure 5. Adiabatic true stress-true strain behavior for the Ti-6Al-4V alloy at a strain rate of 5000 s^{-1} as predicted by the JC material model. Results are presented for loading in tension, compression and shear. The adiabatic temperature rise is also shown in the figure. The failure point along the stress-strain curve is shown for the three stress states.

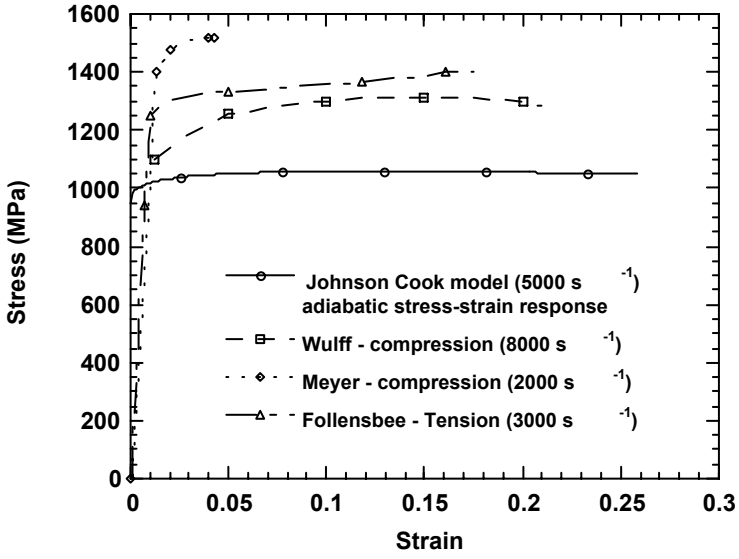

Figure 6. Comparison between the stress-strain behavior predicted by the JC material model and experimental data for the Ti-6Al-4V alloy (obtained from references 11-13).

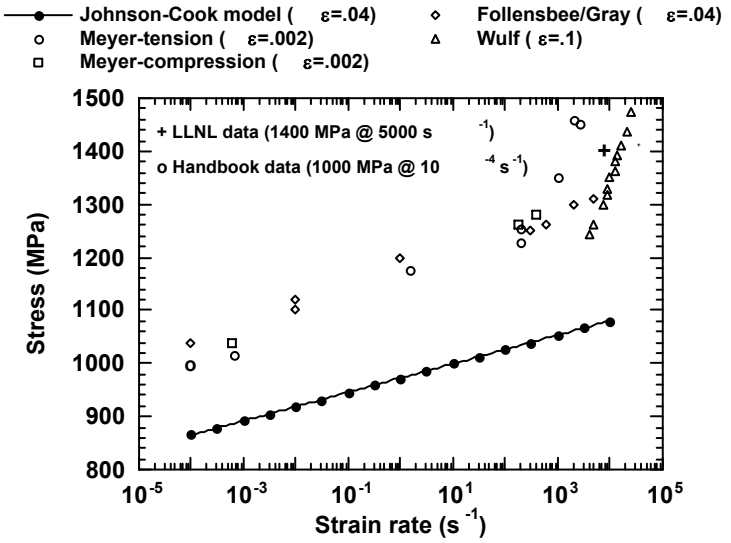

Figure 7. Comparison between the stress-strain rate behavior predicted by the JC material model and experimental data for the 6061-T6 alloy.

Mechanism-Based Material Model

Rate equations

We now derive a rate equation representing deformation that can be controlled by two sequential processes - 1) the cutting (or by-passing) of obstacles by dislocations or 2) the drag on moving dislocations by phonons or electrons. The problem is illustrated schematically in Fig. 8, which shows dislocations in contact with discrete obstacles that have an average spacing d. After Frost and Ashby [14], the average velocity (v) for a dislocation moving through these obstacles is

$$v = d / (t_1 + t_2) \tag{5}$$

where t_1 is the time required to cut or by-pass the obstacle and t_2 is the time spent moving to the next obstacle. Different rate equations represent the deformation kinetics associated with discrete obstacles and drag. Let $\dot{\varepsilon}_1$ represent the strain rate when deformation is

controlled by the cutting (or by-passing) of discrete obstacles, and $\dot{\varepsilon}_2$ represent the strain rate when deformation is controlled by drag on moving dislocations. Since

$$\dot{\varepsilon} = \rho b v \tag{6}$$

where $\dot{\varepsilon}$ is the strain rate, b is the Burger's vector and ρ is the mobile dislocation density,

$$\dot{\varepsilon}_{eff} = \frac{d}{\frac{d}{\dot{\varepsilon}_1} + \frac{d}{\dot{\varepsilon}_2}} \tag{7}$$

where $\dot{\varepsilon}_{eff}$ is the effective strain rate on the slip plane shown in Fig. 8. Thus

$$\dot{\varepsilon}_{eff} = \frac{\dot{\varepsilon}_1 \dot{\varepsilon}_2}{\dot{\varepsilon}_1 + \dot{\varepsilon}_2} \tag{8}$$

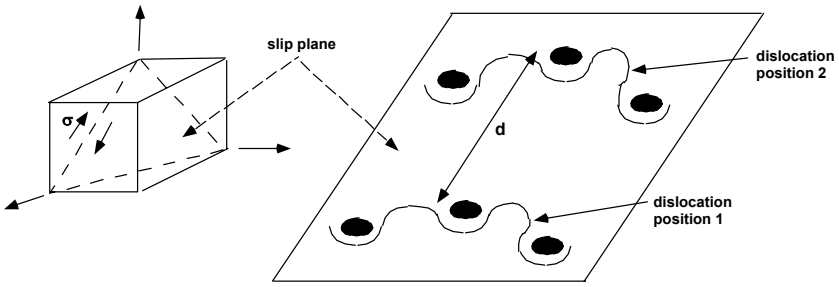

Figure 8. Dislocations on a slip plane in contact with discrete obstacles. The shear stress on the slip plane is σ and the average spacing between obstacles is d. At high strain rates, the dislocation velocity (and therefore strain rate) is determined by the rate at which the discrete obstacles are bypassed or the rate at which the dislocation moves from one discrete obstacle to the next.

The rate equation for discrete obstacle controlled plasticity [15] can be taken as

$$\dot{\varepsilon}_1 = \dot{\varepsilon}_0 \exp\left[\frac{Q}{kT}\left(1-\frac{\sigma}{\tau}\right)\right] \tag{9}$$

where $\dot{\varepsilon}_0$ is a constant, Q is an activation energy, k is Boltzmann's constant, σ is the stress and τ is the strength of the obstacle at 0K. At constant temperature, the equation can be taken as

$$\dot{\varepsilon}_1 = A\exp(B\sigma) \tag{10}$$

where A and B are constants. The rate equation for phonon or electron drag controlled plasticity can be taken as

$$\dot{\varepsilon}_2 = C\sigma^D \tag{11}$$

where C and D are constants. Several theoretical treatments have shown that D approaches 1 [16, 17]. We will use the general form of the rate equation shown in Eqn (11).

Model evaluation

The model, as represented by Eqns (8), (10) and (11), was evaluated against the stress-strain rate data for the 6061-T6 and Ti-6Al-4V alloys shown in Figs. 4 and 7, respectively. The constants for obstacle controlled plasticity (A and B) were evaluated in the strain rate range where this mechanism is dominant. Similarly, the constants for drag controlled plasticity (C and D) were evaluated in the strain rate range where this mechanism is dominant. Figure 9 shows a comparison of the stress-strain rate response predicted by the mechanism-based material model and experimental data for the 6061-T6 alloy. Similarly, Figure 10 shows a comparison of the stress-strain rate response predicted by the mechanism-based material model and experimental data for the Ti-6Al-4V alloy. The figures also show the regions of the stress-strain curves that are dominated by discrete obstacle plasticity and by drag controlled plasticity. For both alloys, the agreement between the model predictions and experimental data is excellent.

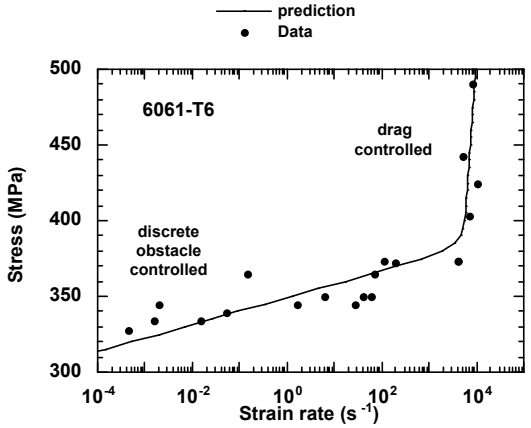

Figure 9. Comparison between the stress-strain rate behavior predicted by the mechanism-based material model and experimental data for the 6061-T6 alloy. The figure shows the regions of the stress-strain rate curve that are dominated by discrete obstacle plasticity and drag controlled plasticity.

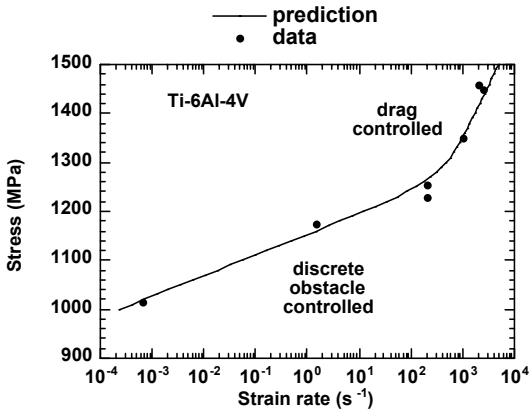

Figure 10. Comparison between the stress-strain rate behavior predicted by the mechanism-based material model and experimental data for the Ti-6Al-4V alloy. The figure shows the regions of the stress-strain rate curve that are dominated by discrete obstacle plasticity and drag controlled plasticity

Gurson Void Growth Model

Observations have been made that ductile fracture in metals is related to the nucleation and growth of voids. Conventional plasticity models, e.g. von Mises, are based on the assumption of plastic incompressibility and can not predict the growth of voids during yielding. Studies have indicated [18-20] that void growth during tensile loading is related to the hydrostatic component of stress and that this porosity increase directly affects material yielding. In these observations it was assumed that the material surrounding a void was incompressible. Gurson proposed [8] a pressure sensitive macroscopic yield surface which relates void growth to the evolution of microscopic (pointwise physical quantities of the matrix material) and macroscopic quantities to account for the behavior of void-containing solids. Here, macroscopic refers to the average values of physical quantities, which represent the material aggregate behavior. As defined by Gurson, the yield surface for a ductile material is:

$$\Phi = \left(\frac{q}{\sigma_o}\right)^2 + 2q_1 f \cosh\left(-\frac{3q_2 p}{2\sigma_o}\right) - (1+q_2 f^2) = 0 \qquad (12)$$

where σ_o is the tensile flow stress of the microscopic matrix material, q and p are the equivalent stress and hydrostatic stresses of the macroscopic material and f is the current void volume

fraction which is a function of the initial porosity, the void growth and nucleation during yielding. The material parameters q_1, q_2 are defined by Gurson. For the current study, the Gurson model was modified to correctly account for the evolution of plastic strain in the micro (matrix) material and to account for strain rate sensitivity. The model was added to the finite element code DYNA3D.

The response of a notched bar under uniaxial tensile loading was simulated to demonstrate the DYNA3D application of the Gurson model. Substantial hydrostatic tension is created in the notched regions of the bar for this type of loading. This hydrostatic stress accelerates void growth and leads to the eventual coalescence of voids and ductile failure of the bar. Failure was assumed to correspond to the loss of load carrying capability in this displacement controlled simulation. The bar was assumed to have the following material properties; E = 20.7 GPa, υ=0.3, yield stress = 690 MPa with a linear hardening modulus of 1,540 MPa. The initial void fraction was assumed to be equal to .050. The initial and deformed shapes of the tensile specimen are shown in Fig. 11, which also depicts the regions of predicted high void growth. The effect of rate dependence is shown in Fig. 12, where an increased loading rate resulted in an increased normalized axial load (actual axial load/initial yield strength), with softening similar to the rate independent Gurson model results. Also shown in Fig. 12 is the conventional plasticity solution, which does not exhibit the pronounced softening predicted by the Gurson model. The conventional plasticity yield surface is also shown to be larger, with a higher strain to failure, than the porous material, a result confirmed by experimental results. For this simulation, the final void fraction was 0.70. A calculation was also performed to check the sensitivity of the solution to mesh size. The mesh in this calculation was twice the density of the initial simulation. The results of this calculation, shown in Fig. 13, indicate that there is some small mesh sensitivity of the solution, in the post failure phase, for the rate independent Gurson solution.

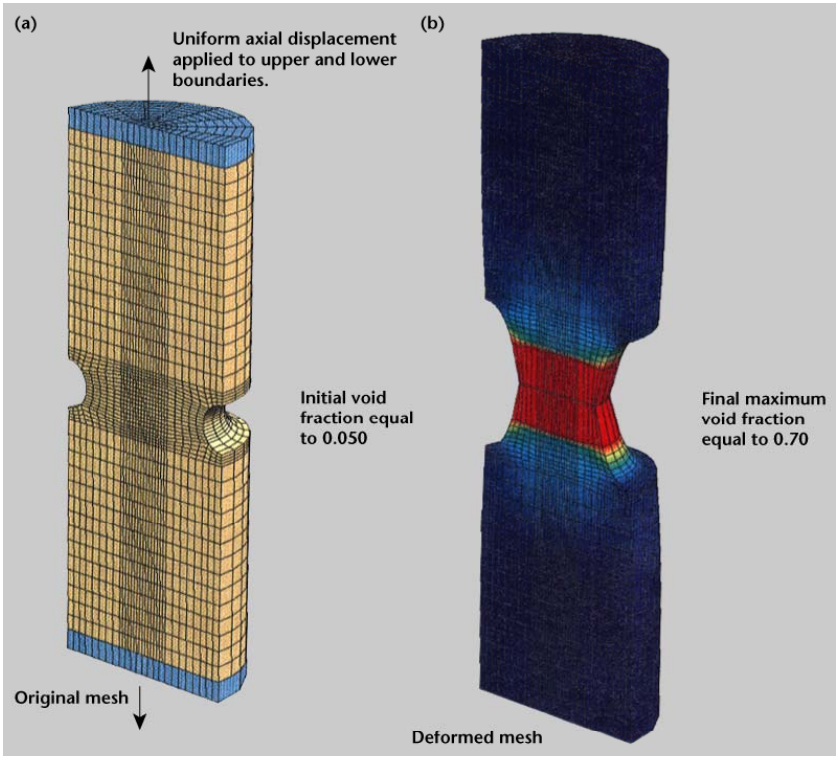

Figure 11. Notched tensile specimen void growth as predicted by the Gurson model. Original mesh is shown in (a) and deformed mesh is shown in (b).

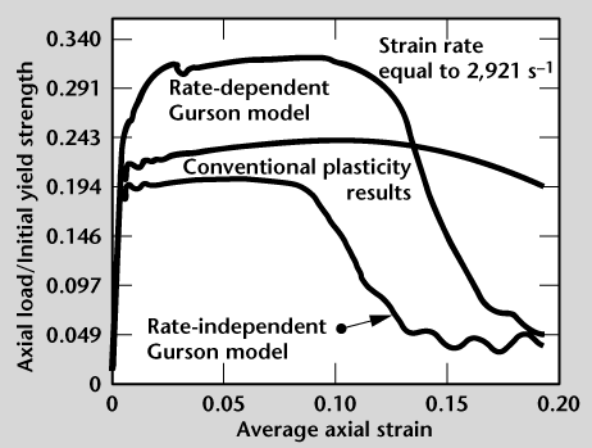

Figure 12. Gurson model rate effects for a notched bar under displacement controlled axial loading.

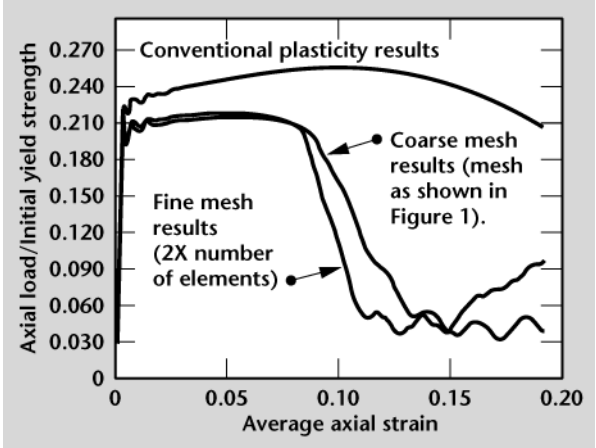

Figure 13. Gurson model mesh sensitivity for a notched bar under displacement controlled axial loading.

Summary

The large strain deformation response of 6061-T6 and Ti-6Al-4V has been evaluated over a range in strain rates from from 10^{-4} s^{-1} to over 10^{4} s^{-1}. The results have been used to critically evaluate the strength and damage components of the JC material model. A new model that addresses the shortcomings of the JC model was then developed and evaluated. The model is derived from the rate equations that represent deformation mechanisms active during moderate and high rate loading. We have also evaluated a model that accounts for the influence of void formation on yield and flow behavior of a ductile metal (the Gurson model). The primary conclusions and observations relative to these three models are as follows.

1. JC model. For the alloys studied, the JC model can accurately represent the yield and work hardening behavior of the materials. The JC model predicts higher failure strains than observed experimentally. The most serious shortcoming of the JC model is its inability to represent the variation of flow stress with strain rate.

2. Deformation mechanism model. This model accounts for two sequential deformation mechanisms that are active at moderate and high deformation rates. The mechanisms are discrete obstacle plasticity and drag controlled plasticity. The model has been developed and evaluated against stress-strain rate data for the 6061-T6 alloy and theTi-6Al-4V alloy. Agreement between experimental results and model predictions is excellent.

3. Gurson void growth model. The Gurson void growth model has been introduced into the DYNA3D code. The model was modified to account for the evolution of plastic strain and strain rate sensitivity. The model was used in the DYNA3D code to simulate the response of a notched bar during tensile loading.

References

1. G. R. Johnson and W. H. Cook, "Fracture Characteristics of Three Metals Subjected to Various Strains, Strain Rates, Temperatures and Pressures", Engineering Fracture Mechanics, 21 (1), (1985), 31-48.

2. G. R. Johnson and W. H. Cook, “A Constitutive Model and Data for Metals

Subjected to Large Strains, High Rates and High Temperatures," in Proceedings of the Seventh International Symposium on Ballistics, The Netherlands: The Hague, 1983, 541-547.
3. G. R. Johnson and T. J. Holmquist, "Evaluation of Cylinder-Impact Test Data for Constitutive Model Constants", Journal of Applied Physics, 64 (8), (1988), 3901-3910.
4. F. J. Zerilli and R. W. Armstrong, "Dislocation-Mechanics-based Constitutive relations for Material Dynamics Calculations", Journal of Applied Physics, 61 (5), (1987), 1816-1825.
5. F. J. Zerilli and R. W. Armstrong, "Description of Tantalum Deformation Behavior by Dislocation Mechanics Based Constitutive Equations", Journal of Applied Physics, 68 (4), (1990), 1580-1591.
6. F. J. Zerilli and R. W. Armstrong, "The Effect of Dislocation Drag on the Stress-Strain Behavior of FCC Metals", Acta Metallurgica et Materialia, 40 (8), (1992), 1803-1808.
7. P. S. Follansbee and U. F. Kocks, "A Constitutive Description of the Deformation of Copper Based on the use of the Mechanical Threshold Stress as an Internal State Variable", Acta Metallurgica, 36 (1988), 81-93.
8. A. J. Gurson, "Continuum Theory of Ductile Rupture by Void Nucleation and Growth Part I - Yield Criteria and Flow Rules for Porous Ductile Media", Journal of Engineering Materials Technology, 99 (1977), 2-15.
9. T. Nicholas, "Tensile Testing of Material at High Rates of Strain", Experimental Mechanics, May 1981 (1981), 177 - 185.
10. P. S. Follansbee, "High-Strain-Rate Deformation of FCC Metals and Alloys," in Metallurgical Applications of Shock-Wave and High-Strain-Rate Phenomena, L. E. Murr, K. P. Staudhammer, and M. A. Meyers, eds. (New York: Marcel Dekker, Inc., 1986), 451 - 479.
11. G. L. Wulf, "High Strain Rate Compression of Titanium and Some Titanium Alloys", International Journal of Mechanical Sciences, 21 (1979), 713 - 718.
12. L. W. Meyer, "Strength and Ductility of a Titanium-Alloy Ti-6Al-4V in Tensile and Compressive Loading Under Low, Medium and High Rates of Strain," in Titanium Science and Technology, G. Lutjering, U. Zwicker, and W. Bunk, eds. (Deutsche Gessellschaft fur Metallkunde, 1984) .
13. P. S. Follansbee and I. G.T. Gray, "An Analysis of the Low Temperature, Low and High Strain-Rate Deformation of Ti-6Al-4V", Metallurgical Transactions *A*, 20A (1989), 863 - 874.
14. H. J. Frost and M. F. Ashby, "Motion of a Dislocation Acted on by a Viscous Drag Through an Array of Discrete Obstacles", Journal of Applied Physics, 42 (13), (1971), 5273 - 5279.
15. H. J. Frost and M. F. Ashby, Deformation Mechanism Maps. Oxford: Pergamon Press, 1982.
16. A. V. Granato, "Microscopic Mechanisms of Dislocation Drag," in Metallurgical Effects at High Strain Rates, (New York: Plenum Press, 1973), 255 - 275.
17. A. Kumar, F. E. Hauser, and J. E. Dorn, "Viscous Drag on Dislocations in Aluminum at High Strain Rates", Acta Metallurgica, 16 (1968), 1189 - 1197.
18. F. A. McClintock, "A Criterion for Ductile Fracture by the Growth of Holes", Journal of Applied Mechanics, 35 (1968), 363-371.
19. J. R. Rice and D. M. Tracy, "On the Ductile Enlargement of Voids in Triaxial Stress Fields", Journal of the Mechanics and Physics of Solids, 17 (1969), 201-217.
20. K. J. Kahlow and B. Avitzur, "Void Behavior as Influenced by Deformation and Pressure," American Iron and Steel Institute, Lehigh University 1969.